iScience

CellPress
OPEN ACCESS

Article

Platelet factors ameliorate thoracic aortic aneurysm and dissection by inhibiting the FGF-FGFR cascade activation in aortic-endothelial cell

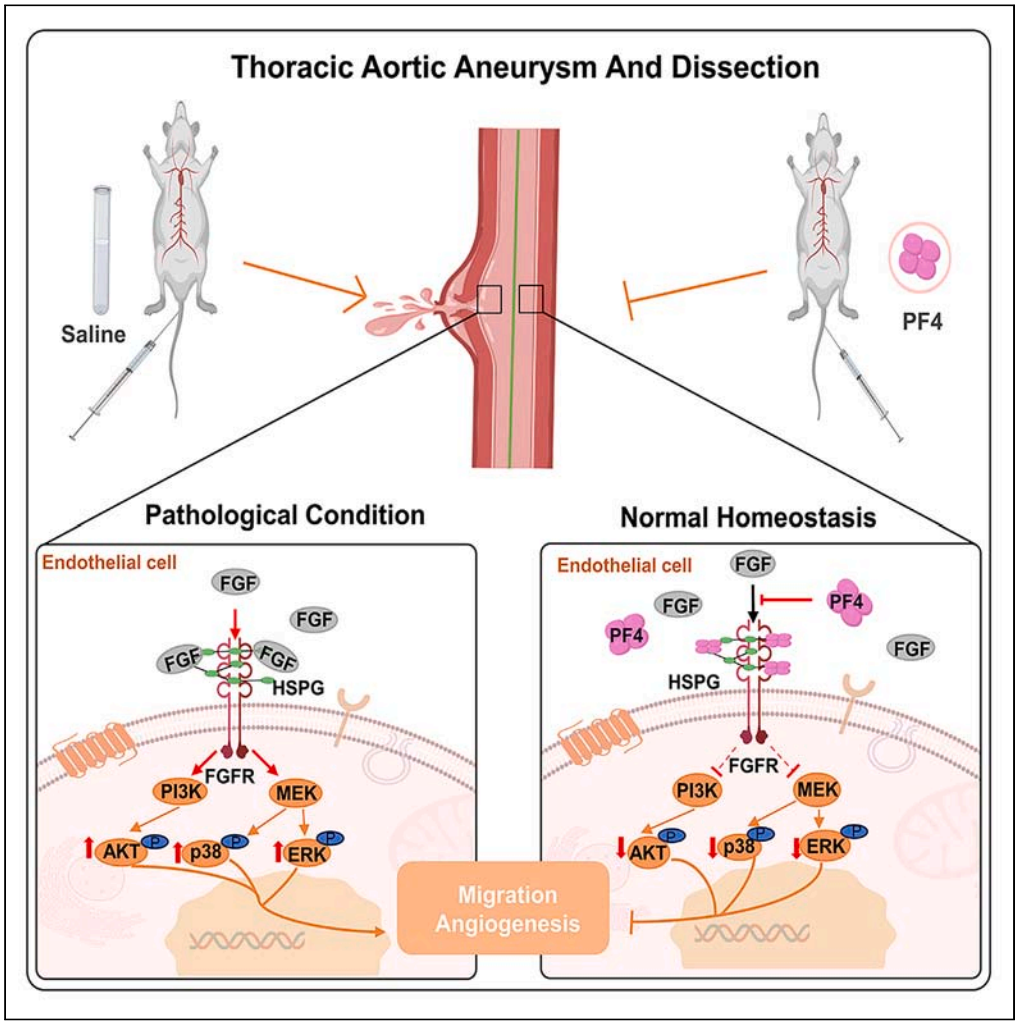

Jizhong Wang, Caiyun He, Yuanwei Chen, ..., Fan Yang, Jie Li, Jianfang Luo

syjieli@sina.com (J.L.)
jianfangluo@sina.com (J.L.)

Highlights

Lipo-PF4 inhibited the development of thoracic aortic aneurysm and dissection

PF4 maintained the endothelial integrity of the aorta effectively in TAAD-mice

PF4 improves endothelial cell function *in vitro* by blocking FGF-FGFR signaling

Wang et al., iScience 27, 110953
October 18, 2024
https://doi.org/10.1016/j.isci.2024.110953

iScience

CellPress
OPEN ACCESS

Article

Platelet factors ameliorate thoracic aortic aneurysm and dissection by inhibiting the FGF-FGFR cascade activation in aortic-endothelial cell

Jizhong Wang,[1,2,7] Caiyun He,[2,7] Yuanwei Chen,[1,2,7] Xiaolu Hu,[1,2] Heng Xu,[5] Jie Liu,[1] Yi Yang,[2] Lang Chen,[2] Ting Li,[2] Lixin Fang,[2,3] Fan Yang,[4] Jie Li,[2,6,*] and Jianfang Luo[2,3,8,*]

SUMMARY

Thoracic aortic aneurysm and dissection (TAAD) is closely associated with vascular endothelial dysfunction. Platelet factor 4 (PF4) is crucial for maintaining vascular endothelial cell homeostasis. However, whether PF4 can influence the progression of TAAD remains unknown. In the present study, we constructed a liposome-encapsulated PF4 nanomedicine and verified its effect on BAPN-induced TAAD *in vivo*. We found that liposome PF4 nanoparticles (Lipo-PF4), more effectively than PF4 alone, inhibited the formation of TAAD. *In vitro*, PF4 improved endothelial cell function under pathological conditions by inhibiting migratory and angiogenic abilities of human aortic endothelial cells (HAECs). Mechanically, PF4 inhibited the development of TAAD and improved HAECs function by combining with heparin sulfate and blocking fibroblast growth factor-fibroblast growth factor receptor (FGF-FGFR) signaling. Taken together, we developed a nano-drug (Lipo-PF4) that effectively ameliorates the progression of TAAD by improving endothelial function. Lipo-PF4 is expected to be a therapeutic option for TAAD in the future.

INTRODUCTION

Thoracic aortic aneurysm and dissection (TAAD) is a highly lethal cardiovascular condition that can lead to sudden death owing to aortic rupture. TAAD refers to dilation or aneurysm of the thoracic aorta, often accompanied by aortic dissection. Various risk factors contribute to the development of TAAD, including underlying genetic predisposition, hypertension, atherosclerosis, aortic diameter, and/or aneurysm.[1] Currently, no pharmacological therapies have been validated as effective in mitigating or preventing the progression of TAAD, despite recent advancements in the surgical repair of TAAD.[2]

To date, the pathogenic mechanisms of TAAD remain elusive. TAAD is characterized by the pathological manifestation of endothelial cell dysfunction, loss of vascular smooth muscle cells (VSMCs), and degradation of elastic fibers in the aortic wall.[3,4] These modifications can result in rupture and death. Tearing of the intima and endothelial cell dysfunction are critical steps in the development of TAAD. Endothelial cell (EC), one of the vital cell types implicated in vascular pathophysiology, have attracted increasing attention in the study of aortic diseases. Recently, Yang et al. reported that endothelial tight junctions' function was disrupted in a β-aminopropionitrile (BAPN)-induced TAAD mouse model through a new type of contrast medium. Furthermore, inhibitors targeting endothelial tight junctions have been shown to reduce the incidence of TAAD. However, the mechanism by which the molecular function of EC is disrupted during TAAD development remains unclear.

Human platelet factor 4 (PF4), also known as chemokine ligand 4 (CXCL4), is a chemokine with a molecular weight of 7.8 kDa. It is primarily synthesized by megakaryocytes and released from platelet α-granules. PF4 primarily exists as a tetramer[5] and has a strong affinity for negatively charged molecules, such as infectious agents[6] and endothelial proteoglycans.[7] It has been reported that PF4 has a significant involvement in various diseases, particularly cardiovascular diseases. Gentilini et al.[8] found that PF4 inhibits human umbilical vein endothelial cell proliferation by interfering with the activity of cyclin E-cyclin-dependent kinase 2 (cdk2). Bikfalvi demonstrated the anti-angiogenic effects of PF4 through three distinct mechanisms.[9]

Despite the crucial role of PF4 in the inhibition of endothelial cell proliferation and angiogenesis, no previous study has explored the potential relationship between PF4 and TAAD. Our study revealed that PF4 can improve TAAD in mice. We constructed liposome-PF4 (Lipo-PF4)

[1]School of Medicine, School of Medicine South China University of Technology, Guangzhou 510000, China
[2]Department of Cardiology, Guangdong Provincial People's Hospital (Guangdong Academy of Medical Sciences), Southern Medical University, Guangzhou 510000, China
[3]Guangdong Cardiovascular Institute, Guangdong Provincial People's Hospital, Guangdong Academy of Medical Sciences, Guangzhou 510000, China
[4]Department of Emergency and Critical Care Medicine, Guangdong Provincial People's Hospital (Guangdong Academy of Medical Sciences), Southern Medical University, Guangzhou 510000, China
[5]Department of Cardiovascular Medicine, Jieyang People's Hospital, Jieyang 522000, China
[6]Linzhi People's Hospital, Xizang 860100, China
[7]These authors contributed equally
[8]Lead contact
*Correspondence: syjieli@sina.com (J.L.), jianfangluo@sina.com (J.L.)
https://doi.org/10.1016/j.isci.2024.110953

to explore the mechanisms by which liposomes improve drug bioavailability and effectiveness.[10] Our findings validated that Lipo-PF4 significantly improved the pathological condition of TAAD.

RESULTS

PF4 improves endothelial cell function under pathological conditions

We treated human aortic endothelial cells (HAECs) with various concentrations of Ang II or TNF-α for 48 h to establish their effective doses. Subsequently, we assessed the proliferation (Figures S1A and S1B) and adhesion abilities of the cells (Figures S1C and S1D). At low concentrations, Ang II stimulated HAEC proliferation, whereas at high concentrations, it inhibited proliferation. Treatment with 1 μM Ang II decreased the cell adhesion rate by 50%. Therefore, we selected 1 μM Ang II as the pharmacological dose for subsequent experiments. Cell proliferation was not affected by low concentrations of TNF-α but was slightly inhibited at high concentrations. When treated with 5 μM TNF-α, the cell adhesion rate decreased by 50%. Therefore, 5 μM was selected as the pharmacological dose of TNF-α for subsequent experiments. We analyzed PF4 levels to address Ang II- or TNF-α-induced endothelial cell dysfunction. We found that increasing the PF4 concentration resulted in a stronger adhesion ability of HAECs (Figures 1A and 1B). In addition, PF4 reduced the migration (Figures 1C and 1D) and inhibited angiogenesis (Figures 1E and 1F) of Ang II- or TNF-α-induced HAECs.

Liposome encapsulates PF4 and reduces its degradation rate in mice

Considering the positive effect of PF4 on improving endothelial cell function *in vitro*, validation of its effectiveness *in vivo* was necessary. By expressing plasmid pET-28a in *E. coli*, we produced and obtained murine-derived PF4 protein. Protein purity was detected by SDS-PAGE with Coomassie brilliant blue staining (Figure S2A). We utilized the well-established lipid film hydration method to encapsulate PF4 into liposomes, which are widely recognized as highly effective nanodrugs. The morphology of the liposomal nanodrugs was examined using an electronic microscope to confirm their formation. Lipo-PF4 samples displayed liposomal structures measuring approximately 100 nm in diameter (Figure 2A). Dynamic light scattering (DLS) analysis revealed that the intensity averaged hydrodynamic diameter of Lipo-PF4 was 100 nm (Figure 2B). Furthermore, we assessed the encapsulation efficiency of the liposomes using an ELISA assay (Figure 2C). In summary, we successfully prepared Lipo-PF4, a systemic drug with a size of approximately 100 nm that can be transported in the bloodstream. Liposomes maintained a higher concentration of PF4 in the blood of mice after 48 h (Figure 2D). After 100 μg/kg PF4 liposome-CY5 was injected into 8-week-old C57 mice for 12 h through the tail vein, the PF4 liposome-CY5 distribution was detected by immunofluorescence. We found that Lipo-PF4 was mainly found in endothelial cells of vascular intima, and a small part was found in smooth muscle cells of vascular media (Figure 2E).

Additionally, we evaluated the biosafety of Lipo-PF4. H&E staining of the liver, heart, spleen, lung, and kidneys of mice after different treatments revealed no histopathological damage (Figure S2B). Next, we measured routine blood indicators, including alanine transaminase (ALT), aspartate transaminase (AST), alkaline phosphatase (ALP), creatinine (CR), and microalbumin (mALB). No statistically significant differences were observed (Figures S2C–S2E). These results demonstrated the biological safety of Lipo-PF4.

Lipo-PF4 nanoparticles ameliorate TAAD formation *in vivo*

Four-week-old mice were then subjected to TAAD induction (4 weeks with BAPN for 21 days and 7 days with AngII) to investigate the potential effect of Lipo-PF4 on the progression of TAAD.[11] Moreover, A BAPN-induced mouse (3 weeks with BAPN for 25 days) TAAD model[12] was established to investigate the potential effect of Lipo-PF4 on the progression of TAAD. The experimental protocol is briefly described in Figures 3A and S3A. The increased aortic diameter of TAAD mice was reduced after treatment with Lipo-PF4 (Figures 3B–3E). However, PF4 had a tendency to decrease the maximum aortic diameter of TAAD mice, but there was no significant statistical difference between PF4 and TAAD mice (Figures 3D and 3E). Lipo-PF4 significantly reduced the incidence of BAPN with AngII-induced TAAD from 70% to 20% (Figure 3F). In addition, Lipo-PF4 significantly reduced the incidence of BAPN-induced TAAD from 70% to 20% (Figure S3B). Lipo-PF4 was more effective in reducing the incidence of TAAD in mice than PF4 (10% vs. 40% and 20% vs. 50%) in both models (Figures 3F and S3B). Lipo-PF4 effectively maintained the endothelial integrity of the aorta in mice (Figures 3G and S3C). In addition, Lipo-PF4 and PF4 decreased MMP activity in cultured supernatant of vascular wall endothelial cells as evidenced by gelatin zymography assay (Figures 3H and S3D). Furthermore, histological staining analysis of the aortic tissue demonstrated that both Lipo-PF4 and PF4 improved the condition of the aorta and decreased elastin disruption (Figures 3I, 3J, S3E, and S3F). Taken together, our data strongly suggested that Lipo-PF4 ameliorated TAAD formation *in vivo*, and its protective effect is obviously better than that of PF4.

PF4 improves endothelial cell function by combining combination with heparin sulfate

We further explored the relative mechanism of PF4 on endothelial cell function to better understand its biological safety and effectiveness in TAAD treatment. Recently, Lord et al. reported that PF4 has a strong affinity for endothelial-derived heparan sulfate chains, which are crucial for signal transduction.[13] We hypothesized that PF4 would improve endothelial cell function by combining with heparin sulfate. HSase has been extensively used for the removal of heparin sulfate from the cell surface, as mentioned in previous studies.[14,15] We observed that HSase addition did not affect the adhesion, invasion, and angiogenesis of Ang II- or TNF-α-stimulated HAECs (Figure 4). However, HSase reversed the cell adhesion effect of PF4 on HAECs (Figures 4A and 4B). PF4 inhibited HAECs invasion; however, this effect was abolished by HSase (Figures 4C and 4D). The tube formation assay demonstrated that HSase reversed the angiogenic effect of PF4 on HAECs. Our findings confirmed that PF4 improved HAECs function via heparin sulfate.

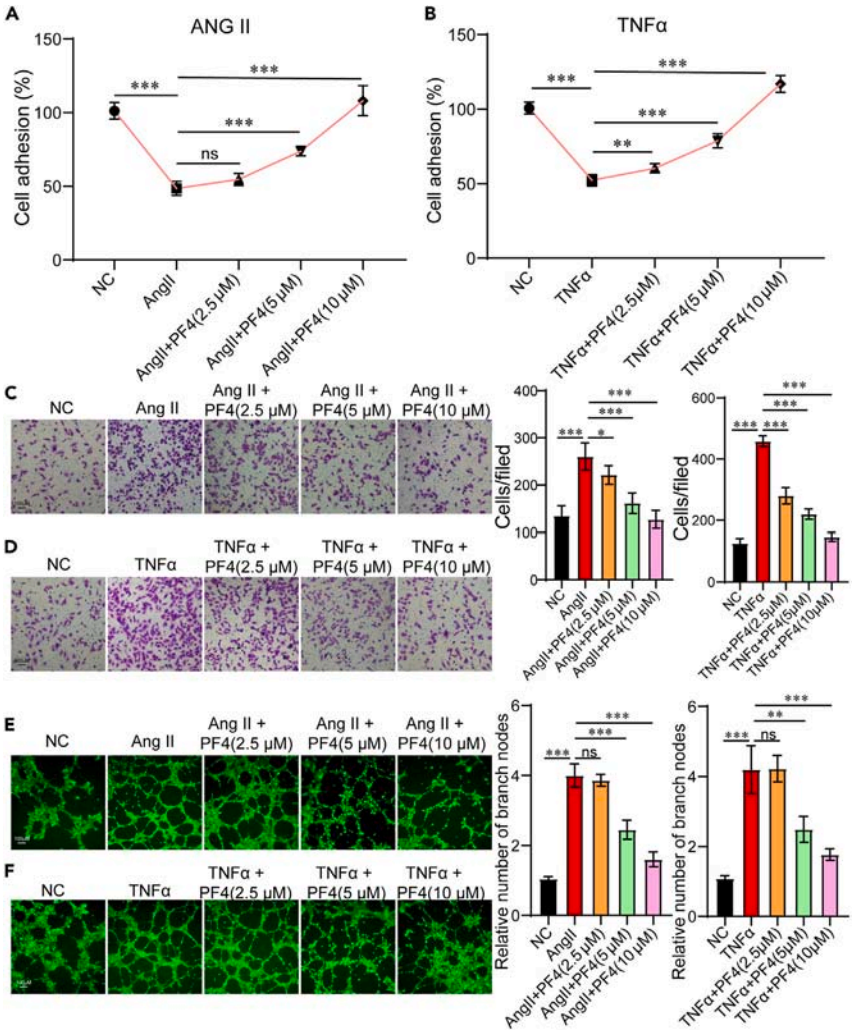

Figure 1. PF4 improves endothelial cell function in pathological conditions

(A) Human aortic endothelial cells were treated with 1 μM AngII alone, 1 μM AngII plus PF4 at the indicated concentrations. Cell adhesion was measured 48 h later using CCK8 assay.

(B) Human aortic endothelial cells were treated with 5 μM TNFα alone, 5 μM TNFα plus PF4 at the indicated concentrations. Cell adhesion was measured 48 h later using CCK8 assay.

(C and D) Human aortic endothelial cells were treated with 1 μM AngII or 5 μM TNFα alone, AngII or TNFα plus PF4 at the indicated concentrations for 36 h, treated cells were seeded onto the upper chamber for 12 h, cells on the lower side of the filter were detected using an inverted microscope.

(E and F) Human aortic endothelial cells were treated with 1 μM AngII or 5 μM TNFα alone, AngII or TNFα plus PF4 at the indicated concentrations for 36 h, treated cells were seeded onto the matrigel for 4 h in a 24-well plate. After incubating with 2 μM calcein AM for 30 min, invert the fluorescence microscope for detection. Data are expressed as mean ± SD. *$p < 0.05$, * *$p < 0.01$, * * *$p < 0.001$.

PF4 inhibits TAAD and improves endothelial cell function by blocking FGF-FGFR signaling

Our findings verified that PF4 improved the function of HAECs via heparin sulfate. However, the precise mechanism by which PF4 interacted with heparin sulfate remained unclear. Structural and biochemical data have revealed that heparan sulfate proteoglycan is required as an additional co-receptor to induce fibroblast growth factor (FGF)-fibroblast growth factor receptor (FGFR) signaling.[16,17] FGF-FGFR signaling has been linked to cell adhesion, angiogenesis, and migration.[18–20] Next, aortic intima was isolated from BAPN group, Lipo-PF4 + BAPN group, and FGFR inhibitor + BAPN group mice for transcriptomic analysis (Figures 5A and S4A). Gene Ontology (GO) pathway enrichment analysis indicated the differentially expressed genes compared between control group and Lipo-PF4 group were enriched in transmembrane receptor protein tyrosine kinase signaling pathway and ERK1 and ERK2 cascade. FGF-FGFR signaling is one of the main members of transmembrane receptor protein tyrosine kinase signaling pathway (Figure 5B). GO pathway enrichment analysis indicated the differentially expressed genes compared between control group and AZD4547 group were enriched in Notch signaling pathway and transmembrane receptor protein tyrosine kinase signaling pathway (Figure S4B). Thus, we inferred that PF4 improved HAECs function by inhibiting FGF-FGFR

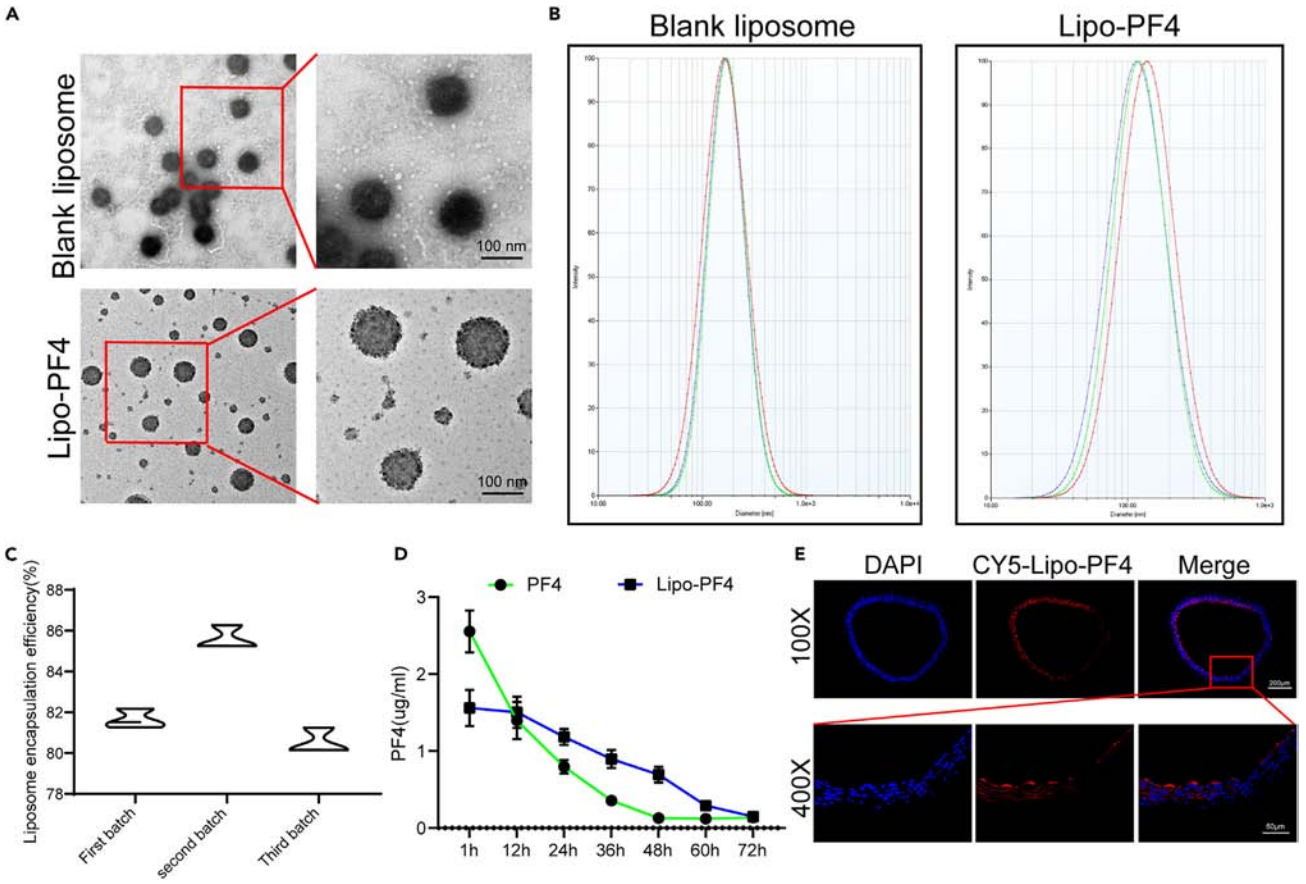

Figure 2. Liposome encapsulation treatment reduces the degradation rate of PF4 protein in mice

(A) PF4-SOD liposome was made through the rotation-evaporation method. Its morphology and diameter were detected using an electronic microscope.

(B) Detection of liposome particle size using dynamic light scattering method.

(C) ELISA assay for detecting the encapsulation efficiency of liposomes.

(D) 100 μg/kg PF4 or PF4 liposome was injected into 8-week-old C57 mice through the tail vein, and the concentration of PF4 in the mouse blood was detected using ELISA assay at different time points.

(E) After 100 μg/kg PF4 liposome-CY5 was injected into 8-week-old C57 mice for 12 h through the tail vein, the PF4 liposome-CY5 distribution was detected by immunofluorescence. Data are expressed as mean ± SD. *$p < 0.05$, * *$p < 0.01$, * * *$p < 0.001$.

activation. However, FGF has some side effects, such as reducing blood pressure and increasing cell proliferation during treatment *in vivo*.[21] SUN11602 was synthesized to mimic the mechanism of basic FGF and overcome the limitations of FGF.[22] We administered SUN11602 with Lipo-PF4 to BAPN-induced mice via the tail vein (Figure 5C). SUN11602 reversed the protective effect of Lipo-PF4 against TAAD. The maximum diameter and incidence of TAAD increased after the addition of SUN11602 compared with the Lipo-PF4 group (Figures 5D–5F). SUN11602 worsened the pathological condition of the aorta in BAPN-induced mice compared to that in the Lipo-PF4 group, as evidenced by the results of H&E, Masson, EVG staining, and gelatin zymography (Figures 5H–5G). Additionally, immunofluorescence staining revealed that HAEC integrity was disrupted in the Lipo-PF4 + SUN11602 group (Figure 5J).

SUN11602 decreased HAEC adherence and increased migratory and angiogenic capacity. SUN11602 reversed the effect of PF4 on the adhesion, migration, and angiogenic capacity of HAECs (Figures S5A–S5F). These results demonstrated that PF4 inhibited the development of TAAD and improved HAECs function by blocking the FGF-FGFR signaling pathway.

PF4 blocks the downstream signal transduction induced by FGF-FGFR

The FGF-FGFR signaling pathway is involved in the regulation of various cellular functions, including migration, differentiation, and proliferation.[23] The classical downstream signaling pathways of FGF-FGFR include PI3K/AKT, Ras/Raf-MEK-MAPK, and STAT signaling pathways.[24] Our findings confirmed that PF4 inhibited TAAD in mice and improved endothelial cell function by blocking FGF-FGFR signaling. However, the effect of PF4 on the FGF-FGFR downstream signaling pathway in HAECs remained to be determined. Western blot analysis revealed that PF4 decreased the expression of phosphorylated (p)-ERK1/2, phosphorylated (p)-P38, and phosphorylated (p)-AKT (Ser473) in Ang II- or

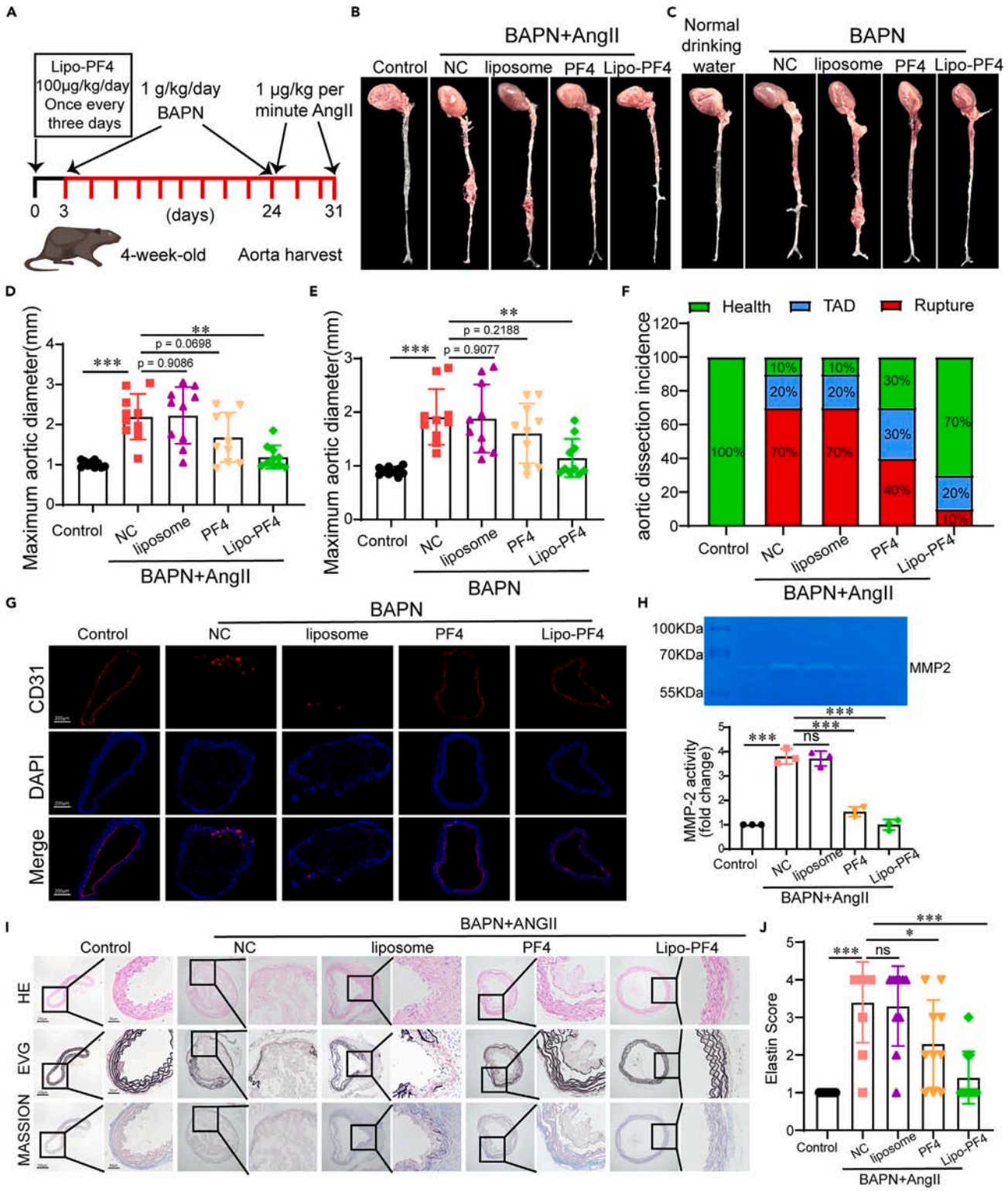

Figure 3. Liposome-PF4 nanoparticles repress thoracic aortic dissection formation by improving endothelial function

(A) Mice were treated with liposome-PF4, PF4, or empty liposome once every three days at 4 weeks. Three days after the first administration, mice were treated with 0.25% BAPN (β-aminopropionitrile monofumarate) for 21 days. Subsequently, mice were treated with 1 μg/kg per minute AngII using minipump (n = 10, per group).

Figure 3. *Continued*

(B and C) Representative images of mice aorta were shown.

(D and E) maximum aortic diameter was measured (n = 10, per group).

(F) AD incidence was statistically analyzed.

(G) Representative images of mouse aorta stained with CD31 (red) and DAPI (blue).

(H) Effect of PF4 on MMP activities in cultured supernatant of vascular wall endothelial cells by gelatin zymography.

(I) Representative macroscopic images of aorta sections were stained with hematoxylin and eosin (H&E), Masson, and elastic-Van Gieson (EVG) staining.

(J) Quantification of elastin integrity in each group of mouse aortas. Data are expressed as mean ± SD. *$p < 0.05$, * *$p < 0.01$, * * *$p < 0.001$.

TNF-α-stimulated HAECs (Figures 6A and 6B). However, these inhibitory effects were abolished by SUN11602 (Figures 6C and 6D) and HSase (Figures S6A and S6B). Collectively, these findings revealed that PF4 blocked the downstream signaling pathways of FGF-FGFR.

DISCUSSION

Our study provides the evidence that PF4 attenuates TAAD development in a mouse model. Elevated circulating levels of PF4 injected into the tail vein significantly reduced the incidence and dilatation of TAAD. Additionally, it maintained the integrity of the endothelial cells and improved the condition of the aorta. Treatment of HAECs with appropriate concentrations of PF4 mitigated Ang II- or TNF-α-induced reduction in cellular adhesion and increased cell migration and angiogenesis by blocking FGF-FGFR signaling. These findings suggest that PF4 may play a role in reducing the development of TAAD, at least in part, through maintaining endothelial cell integrity and improving endothelial function.

PF4, the first isolated chemokine with biological function, is involved in various diseases, including immune thrombocytopenia,[25] age-related cognitive decline,[26] cancer,[27] and atherosclerosis.[28] A recent proteomics study[29] identified PF4 as a potential biomarker for the pathogenesis of aortic dissection. In addition, Xavier et al.[30] revealed the involvement of platelet-derived PF4 and neutrophil-derived IL-8 in the formation of intraluminal thrombus in abdominal aortic aneurysm. Ample evidence suggests a potential association between PF4 and aortic disease; however, no study has been conducted to explore this relationship. The present study demonstrated that PF4 attenuates TAAD formation by improving endothelial cell function. Moreover, the constructed nanoparticle drug containing PF4 exhibited a remarkable protective effect *in vivo*, offering a perspective for the application of PF4. The nanoparticle drug decreased the biodegradability rate of PF4 and was safe *in vivo*, as previously demonstrated for other nanoparticle drugs.[31–33]

Recently, many studies have revealed that endothelial cell barrier dysfunction is a critical characteristic of TAAD progression. Endothelial tight junction disruption, vascular inflammation, and edema have been observed in the aorta of BAPN-induced TAAD.[34] Shanshan et al. reported that the endothelial HDAC1-ZEB2-NuRD complex drives aortic aneurysm[35] and dissection by regulating protein S-sulfhydration.[36] Our findings revealed that PF4 maintains endothelial cell integrity, to alleviate the formation of TAAD *in vivo*. This finding further confirms the significance of endothelial cells in the development of TAAD.[36] Cell migration and tube formation have been identified as characteristic features of aortic dissection. PF4 inhibited the migration and tube formation of HAECs but strengthened cell adhesion. We used a cell adhesion assay to evaluate endothelial cell function in TAAD, which provides an approach for validating cellular functions in TAAD.

Previous studies have discovered relevant molecular mechanisms of PF4 in cardiovascular diseases. Sachais et al. found that PF4 could promote atherosclerosis in mice.[37] Yu et al. discovered that PF4 could increase the expression of E-selectin in endothelial cells through activation of transcriptional activity of nuclear factor-kappa B.[38] Aidoudi and Bikfalvi summarized the proatherogenic role of PF4. PF4 deposited on impaired endothelial cells, recruited peripheral monocytes, and facilitated its differentiation into macrophages, leading to localized inflammation and plaque formation.[39] TAA shares most of the pathogenic mechanisms with atherosclerosis. However, we demonstrated that PF4 protects TAAD formation through maintaining the integrity of endothelial cells *in vivo*. TAAD, as distinguished from atherosclerosis, is characterized by intimal tearing, and false lumen formation. It had been proved that endothelial cell loss and subsequent exposure of subendothelial basement occurred before intimal tearing.[40,41] We surprisingly discovered that PF4 could maintain the integrity of endothelial cells *in vivo* and enhance the adhesion of endothelial cells *in vitro*. We inferred that the effect of PF4 on endothelial cells prevents intimal tearing and protects TAAD formation. Further in-depth studies should be conducted to investigate the converse effect of PF4 between TAAD and atherosclerosis.

The multimerized form of PF4 exerts its pharmacological effects through several mechanisms. PF4 has been proven in studies to effectively inhibit FGF2-induced proliferation of capillary endothelial cells in the adrenal cortex.[42] PF4 inhibits FGF-2 dimerization, contributing to its anti-angiogenic properties in murine microvascular endothelial cells.[43] Our findings validated that PF4 effectively inhibits the migration and angiogenesis of HAECs, while simultaneously improving cell adhesion by blocking FGF-FGFR signaling. We also assessed the effects of PF4 on the downstream signaling of FGF-FGFR.

A previous study indicated that PF4 significantly inhibits ERK phosphorylation, with no effect on Akt phosphorylation.[42] PF4 increases the expression of phosphorylated-P38, as previously reported.[44,45] However, our findings revealed that PF4 decreased the expression of phosphorylated (p)-ERK1/2, phosphorylated (p)-P38, and phosphorylated (p)-AKT (Ser473) in Ang II- or TNF-α-stimulated HAECs. We inferred that these discrepancies could be attributed to the different stimulations and cell types, implying that further in-depth investigations into the mechanism of PF4 and its signaling pathways are necessary.

In conclusion, the present study demonstrated that PF4 has a protective effect against the development of TAAD. PF4 improves endothelial cell adhesion and inhibits cell migration and angiogenesis. These effects were attributed, at least partially, to the inhibition of

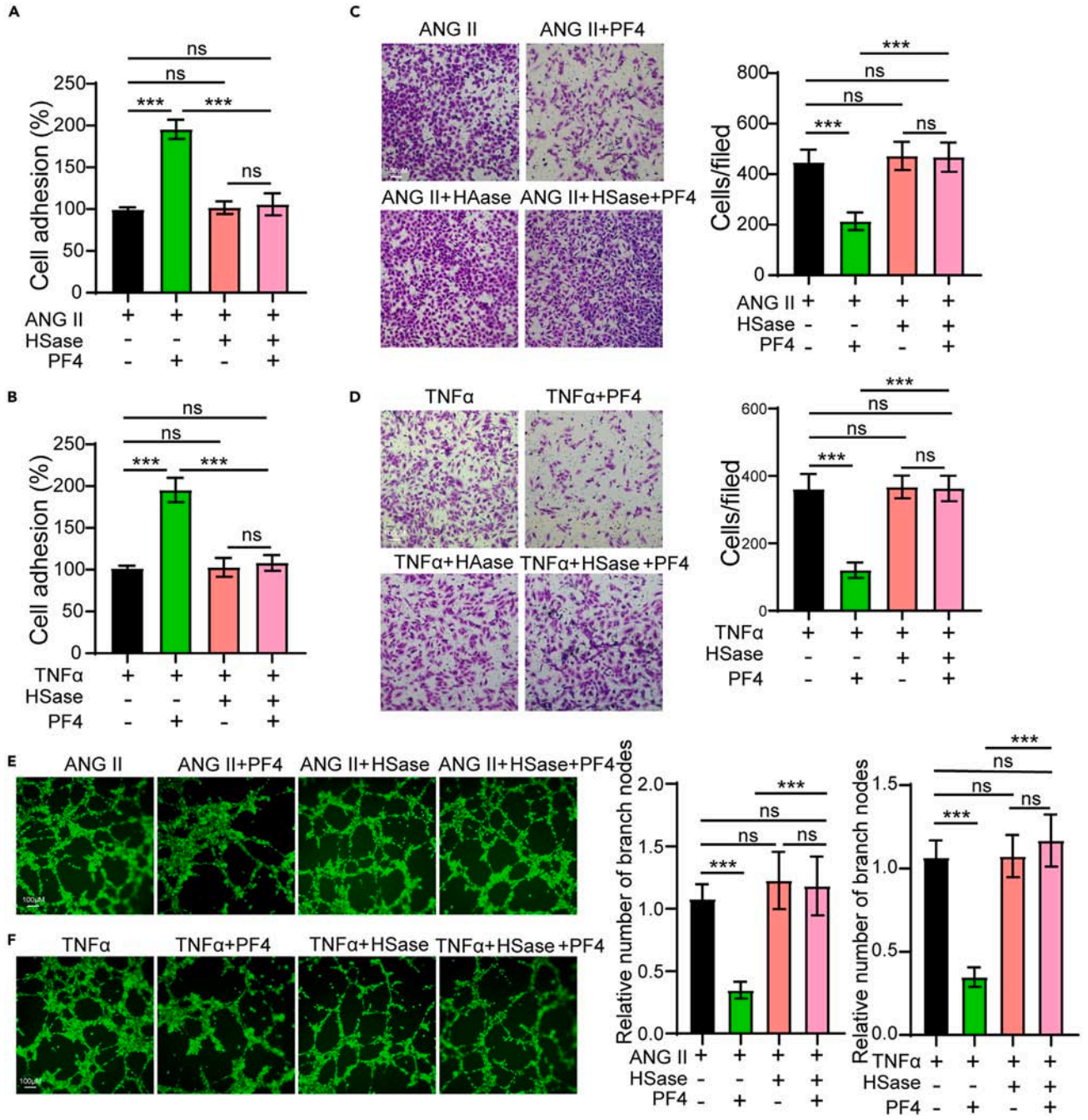

Figure 4. PF4 improves endothelial cell function by combining with heparin sulfate

(A and B) After incubated with HSase (1 mU/ml, Sigma-Aldrich) for 4 h, cells were treated with 1 μM AngII or 5 μM TNFα alone, AngII or TNFα plus PF4 (10 μM) for 48 h, Cell adhesion was measured using CCK8 assay.

(C and D) After incubated with HSase (1 mU/ml, Sigma-Aldrich) for 4 h, cells were treated with 1 μM AngII or 5 μM TNFα alone, AngII or TNFα plus PF4 (10 μM) for 36 h, treated cells were seeded onto the upper chamber for 12 h, cells on the lower side of the filter were detected using an inverted microscope.

(E and F) After incubated with HSase (1 mU/ml, Sigma-Aldrich) for 4 h, cells were treated with 1 μM AngII or 5 μM TNFα alone, AngII or TNFα plus PF4(10 μM) for 36 h, treated cells were seeded onto the matrigel for 4 h in a 24-well plate. After incubating with 2 μM calcein AM for 30 min, the vascular cyclization ability of cells is detected. Data are expressed as mean ± SD. *$p < 0.05$, * *$p < 0.01$, * * *$p < 0.001$.

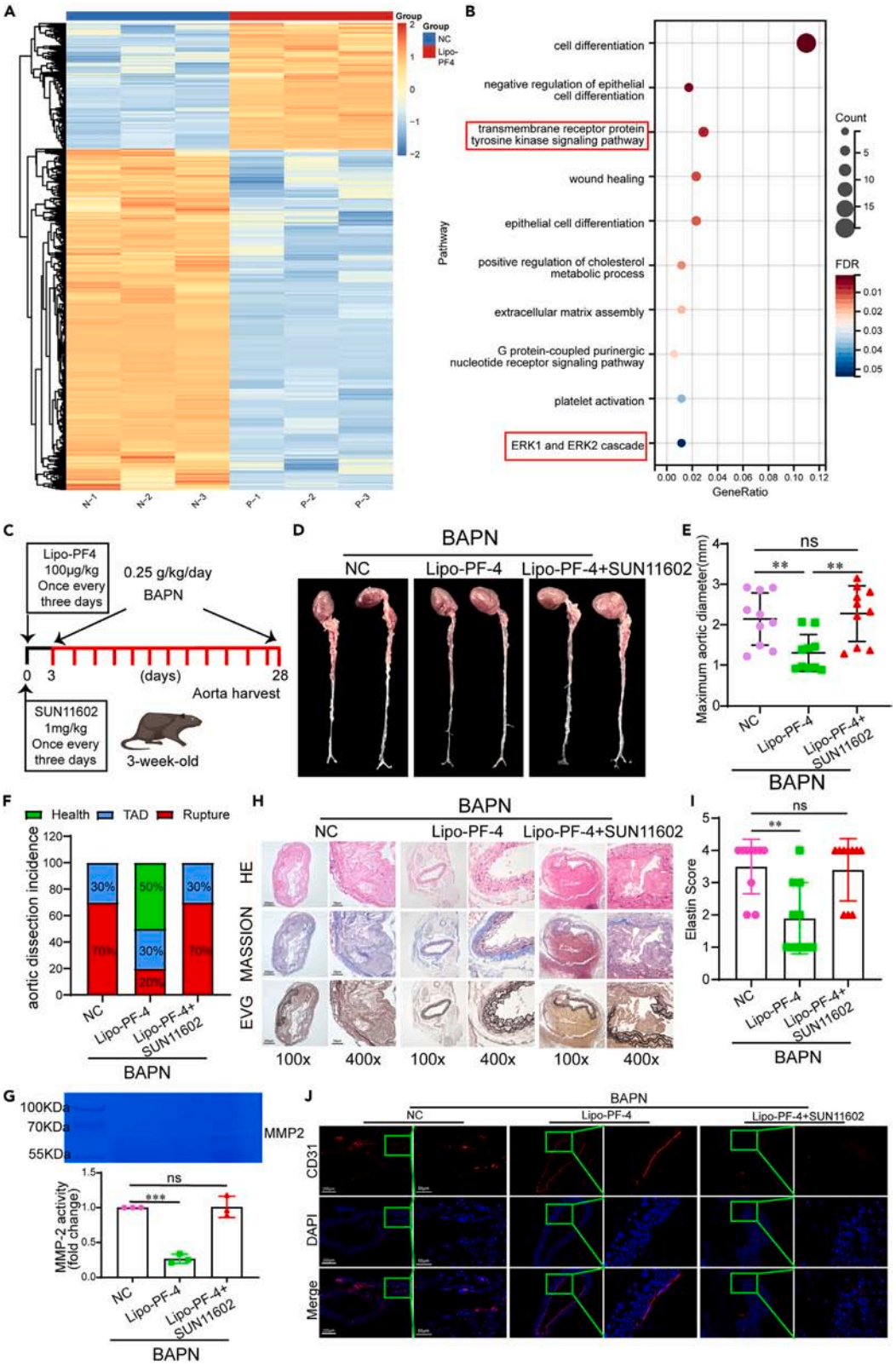
A
Group
NC
Lipo-PF4
N-1
N-2
N-3
P-1
P-2
P-3
B
cell differentiation
negative regulation of epithelial cell differentiation
transmembrane receptor protein tyrosine kinase signaling pathway
wound healing
epithelial cell differentiation
positive regulation of cholesterol metabolic process
extracellular matrix assembly
G protein-coupled purinergic nucleotide receptor signaling pathway
platelet activation
ERK1 and ERK2 cascade
Pathway
GeneRatio
Count
FDR
C
Lipo-PF4 100μg/kg Once every three days
0.25 g/kg/day BAPN
0 3 (days) 28
Aorta harvest
SUN11602 1mg/kg Once every three days
3-week-old
D
BAPN
NC
Lipo-PF-4
Lipo-PF-4+SUN11602
E
Maximum aortic diameter(mm)
ns
**
**
NC
Lipo-PF-4
Lipo-PF-4+ SUN11602
BAPN
F
Health
TAD
Rupture
aortic dissection incidence
30%
50%
30%
70%
30%
70%
20%
NC
Lipo-PF-4
Lipo-PF-4+ SUN11602
BAPN
H
BAPN
NC
Lipo-PF-4
Lipo-PF-4+SUN11602
HE
MASSION
EVG
100x
400x
100x
400x
100x
400x
I
ns
**
Elastin Score
NC
Lipo-PF-4
Lipo-PF-4+ SUN11602
BAPN
G
100KDa
70KDa
55KDa
MMP2
ns
***
MMP-2 activity (fold change)
NC
Lipo-PF-4
Lipo-PF-4+ SUN11602
BAPN
J
BAPN
NC
Lipo-PF-4
Lipo-PF-4+SUN11602
CD31
DAPI
Merge

Figure 5. PF4 represses thoracic aortic dissection formation and improves endothelial cell function by inhibiting the activation of FGF-FGFR

(A) Differential gene analysis between BAPN group and Lipo-PF4 group. Mice were treated with liposome-PF4 once every three days at 3 weeks. Three days after the first administration, mice were treated with 0.25% BAPN (β-aminopropionitrile monofumarate) for 14 days (n = 9, per group).Mouse aortic intima were isolated, and the aortic intima of three mice were mixed into one sample for transcriptome sequencing, and performed differential gene analysis. N: BAPN group; P: lipo-PF4+BAPN group.

(B) GO analysis of differential genes.

(C) Mice were treated with liposome-PF4 or liposome-PF4 plus SUN11602 once every three days at 3 weeks. Three days after the first administration, mice were treated with 0.25% BAPN (β-aminopropionitrile mono fumarate) for 25 days (n = 10, per group).

(D) Representative images of mice aorta were shown.

(E) Maximum aortic diameter was measured (n = 10, per group).

(F) AD incidence was statistically analyzed.

(G) Effect of PF4 and SUN11602 on MMP activities in cultured supernatant of vascular wall endothelial cells by gelatin zymography.

(H) Representative macroscopic images of aorta sections were stained with hematoxylin and eosin (H&E), Masson, and elastic-Van Gieson (EVG) staining.

(I) Quantification of elastin integrity in each group of mouse aortas.

(J) Representative images of mouse aorta stained with CD31 (red) and DAPI (blue). Data are expressed as mean ± SD. *$p < 0.05$, * *$p < 0.01$, * * *$p < 0.001$.

the FGF-FGFR signaling pathway and that it ameliorated TAAD development. Therefore, PF4 may serve as promising therapeutic approach for the prevention and treatment of TAAD.

Limitations of the study

Despite these significant and findings, the present study has several limitations. In this study, we used two types of TAAD model, and the scope of application of PF4 should be clarified through further investigation. Clinical data on the association between PF4 and TAAD prevalence are lacking. Further clinical studies are required to explore the relationship between PF4 and TAAD. Furthermore, the present *in vivo* study was validated by the systemic administration of PF4. Therefore, loss-of-function experiments are required to elucidate the role of endogenous PF4 in TAAD.

RESOURCE AVAILABILITY

Lead contact

Further information and requests for resources and reagents should be directed to and will be fulfilled by the lead contact, Dr Jianfang Luo (jianfangluo@sina.com).

Materials availability

Materials used in this study are available from the lead contact upon reasonable request.

Data and code availability

- The deposited data of this study are presented in key resources table. The data of the RNA-seq (SRA code PRJNA112618061) was deposited to the NIH SRA database. All data reported in this paper will be shared by the lead contact upon reasonable request.
- This paper does not report original code.
- Any additional information required to reanalyze the data reported in this paper is available from the lead contact upon reasonable request.

ACKNOWLEDGMENTS

This study is supported by the National Natural Science Foundation of China (grant 82070478), Guangdong Provincial Clinical Research Center for Cardiovascular Disease (grant 2020B1111170011), and Tibet Autonomous Region Natural Science Foundation (XZ2024ZR-ZY088(Z)).

AUTHOR CONTRIBUTIONS

Conceptualization, J. Luo and J. Li; methodology, J.W., C.H., and Y.C.; Investigation, J.W., C.H., Y.C., X.H., H.X., J. Liu, Y.Y., L.C., and T.L.; data curation, J. Luo and J.Li; writing – original draft, Y.C.; writing – review & editing, J.W. and J. Luo; funding acquisition, J. Luo and J. Li; supervision, J. Luo, J. Li, L.F., and F.Y. project administration, J. Luo and J. Li.

DECLARATION OF INTERESTS

The authors declare no competing interests.

STAR★METHODS

Detailed methods are provided in the online version of this paper and include the following:

- KEY RESOURCES TABLE
- EXPERIMENTAL MODEL AND PARTICIPANT DETAILS
  - Animals
  - Cells
- METHOD DETAILS

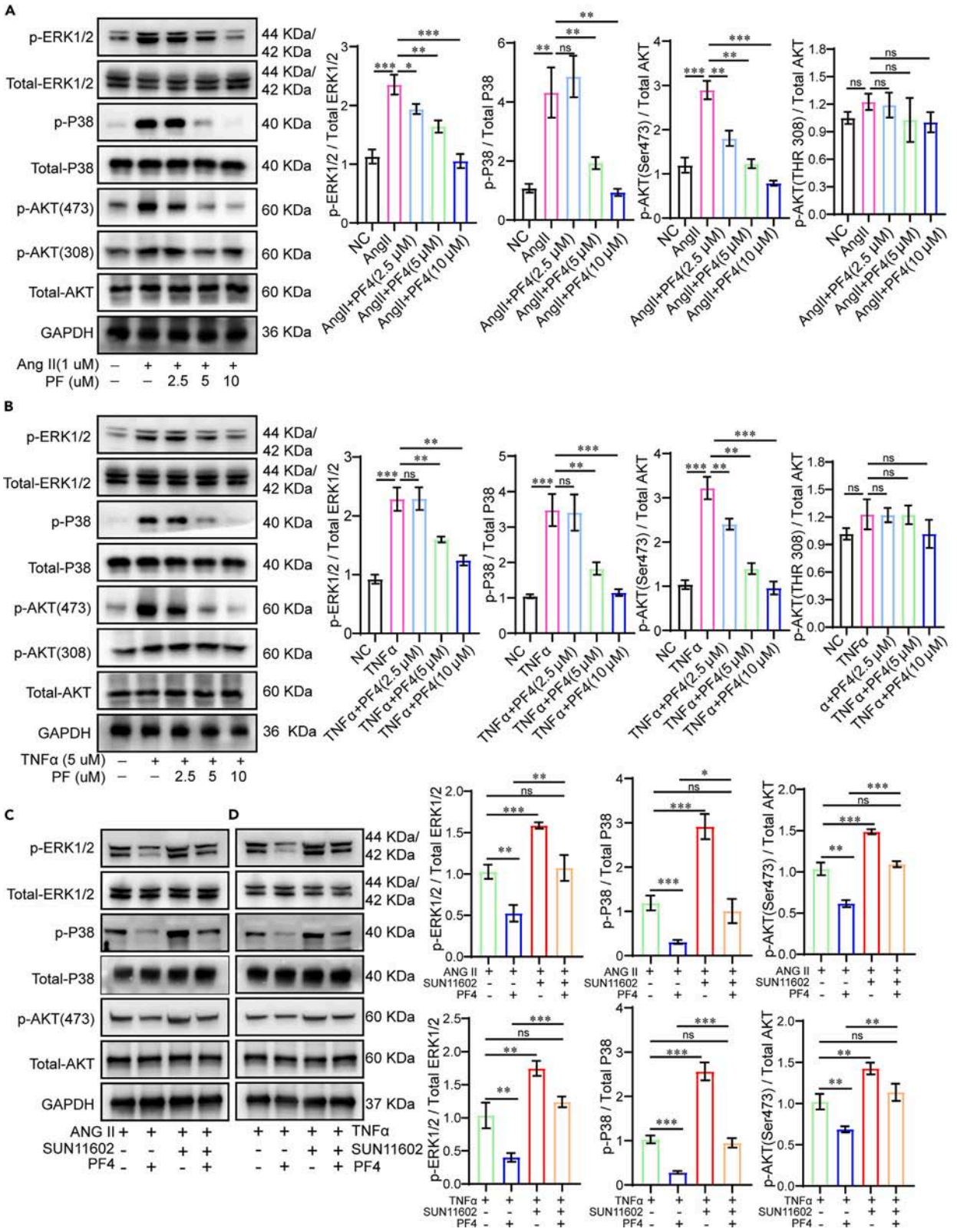
A
p-ERK1/2
Total-ERK1/2
p-P38
Total-P38
p-AKT(473)
p-AKT(308)
Total-AKT
GAPDH
44 KDa/ 42 KDa
40 KDa
60 KDa
36 KDa
Ang II(1 uM)
PF (uM)
p-ERK1/2 / Total ERK1/2
p-P38 / Total P38
p-AKT(Ser473) / Total AKT
p-AKT(THR 308) / Total AKT
NC
AngII
AngII+PF4(2.5 μM)
AngII+PF4(5 μM)
AngII+PF4(10 μM)
B
TNFα (5 uM)
PF (uM)
TNFα
TNFα+PF4(2.5 μM)
TNFα+PF4(5 μM)
TNFα+PF4(10 μM)
C
D
37 KDa
ANG II
SUN11602
PF4
TNFα

Figure 6. PF4 represses MAPK signal transduction by blocking FGFs-FGFR

(A and B) Human aortic endothelial cells were treated with 1 μM AngII or 5 μM TNFα alone, 1 μM AngII or 5 μM TNFα plus PF4 at the indicated concentrations for 24 h. The phosphorylated and total levels of Erk1/2, P38, Akt (Ser 473), and Akt (Thr 308) were detected by western blotting analysis (n = 3).

(C and D) Cells were treated with 1 μM AngII or 5 μM TNFα alone, AngII or TNFα plus PF4(10 μM) and SUN11602(10 μM) for 24 h. The phosphorylated and total levels of Erk1/2, P38, and Akt (Ser 473) were detected by western blotting analysis (n = 3). Density ratios of phosphorylated proteins to total proteins were presented as the mean ± standard deviation. *p < 0.05, * *p < 0.01, * * *p < 0.001.

- Cell proliferation and adhesion assays
- Cell migration assay
- Tube formation assay
- ELISA assays
- Platelet factor 4 protein expression and purification
- Preparation and property analysis of liposomes
- Histological and immunofluorescence staining
- Gelatin zymography
- RNA sequencing
- Western blot

● QUANTIFICATION AND STATISTICAL ANALYSIS

SUPPLEMENTAL INFORMATION

Supplemental information can be found online at https://doi.org/10.1016/j.isci.2024.110953.

Received: March 4, 2024
Revised: June 25, 2024
Accepted: September 10, 2024
Published: September 13, 2024

REFERENCES

1. Pinard, A., Jones, G.T., and Milewicz, D.M. (2019). Genetics of Thoracic and Abdominal Aortic Diseases. Circ. Res. *124*, 588–606. https://doi.org/10.1161/circresaha.118.312436.
2. Famularo, M., Meyermann, K., and Lombardi, J.V. (2017). Aneurysmal degeneration of type B aortic dissections after thoracic endovascular aortic repair: A systematic review. J. Vasc. Surg. *66*, 924–930. https://doi.org/10.1016/j.jvs.2017.06.067.
3. Isselbacher, E.M. (2005). Thoracic and abdominal aortic aneurysms. Circulation *111*, 816–828. https://doi.org/10.1161/01.Cir.0000154569.08857.7a.
4. Halushka, M.K., Angelini, A., Bartoloni, G., Basso, C., Batoroeva, L., Bruneval, P., Buja, L.M., Butany, J., d'Amati, G., Fallon, J.T., et al. (2016). Consensus statement on surgical pathology of the aorta from the Society for Cardiovascular Pathology and the Association For European Cardiovascular Pathology: II. Noninflammatory degenerative diseases - nomenclature and diagnostic criteria. Cardiovasc. Pathol. *25*, 247–257. https://doi.org/10.1016/j.carpath.2016.03.002.
5. Cai, Z., Yarovoi, S.V., Zhu, Z., Rauova, L., Hayes, V., Lebedeva, T., Liu, Q., Poncz, M., Arepally, G., Cines, D.B., and Greene, M.I. (2015). Atomic description of the immune complex involved in heparin-induced thrombocytopenia. Nat. Commun. *6*, 8277. https://doi.org/10.1038/ncomms9277.
6. Gray, A.L., Karlsson, R., Roberts, A.R.E., Ridley, A.J.L., Pun, N., Khan, B., Lawless, C., Luís, R., Szpakowska, M., Chevigné, A., et al. (2023). Chemokine CXCL4 interactions with extracellular matrix proteoglycans mediate widespread immune cell recruitment independent of chemokine receptors. Cell Rep. *42*, 111930. https://doi.org/10.1016/j.celrep.2022.111930.
7. Stringer, S.E., and Gallagher, J.T. (1997). Specific binding of the chemokine platelet factor 4 to heparan sulfate. J. Biol. Chem. *272*, 20508–20514. https://doi.org/10.1074/jbc.272.33.20508.
8. Gentilini, G., Kirschbaum, N.E., Augustine, J.A., Aster, R.H., and Visentin, G.P. (1999). Inhibition of human umbilical vein endothelial cell proliferation by the CXC chemokine, platelet factor 4 (PF4), is associated with impaired downregulation of p21(Cip1/WAF1). Blood *93*, 25–33.
9. Bikfalvi, A. (2004). Platelet factor 4: an inhibitor of angiogenesis. Semin. Thromb. Hemost. *30*, 379–385. https://doi.org/10.1055/s-2004-831051.
10. Bulbake, U., Doppalapudi, S., Kommineni, N., and Khan, W. (2017). Liposomal Formulations in Clinical Use: An Updated Review. Pharmaceutics *9*, 12. https://doi.org/10.3390/pharmaceutics9020012.
11. Zhou, C., Lin, Z., Cao, H., Chen, Y., Li, J., Zhuang, X., Ma, D., Ji, L., Li, W., Xu, S., et al. (2022). Anxa1 in smooth muscle cells protects against acute aortic dissection. Cardiovasc. Res. *118*, 1564–1582. https://doi.org/10.1093/cvr/cvab109.
12. Ren, W., Liu, Y., Wang, X., Jia, L., Piao, C., Lan, F., and Du, J. (2016). β-Aminopropionitrile monofumarate induces thoracic aortic dissection in C57BL/6 mice. Sci. Rep. *6*, 28149. https://doi.org/10.1038/srep28149.
13. Lord, M.S., Cheng, B., Farrugia, B.L., McCarthy, S., and Whitelock, J.M. (2017). Platelet Factor 4 Binds to Vascular Proteoglycans and Controls Both Growth Factor Activities and Platelet Activation. J. Biol. Chem. *292*, 4054–4063. https://doi.org/10.1074/jbc.M116.760660.
14. Dong, W., Lu, W., McKeehan, W.L., Luo, Y., and Ye, S. (2012). Structural basis of heparan sulfate-specific degradation by heparinase III. Protein Cell *3*, 950–961. https://doi.org/10.1007/s13238-012-2056-z.
15. Laboux, T., Maanaoui, M., Allain, F., Boulanger, E., Denys, A., Gibier, J.B., Glowacki, F., Grolaux, G., Grunenwald, A., Howsam, M., et al. (2023). Hemolysis is associated with altered heparan sulfate of the endothelial glycocalyx and with local complement activation in thrombotic microangiopathies. Kidney Int. *104*, 353–366. https://doi.org/10.1016/j.kint.2023.03.039.
16. Chen, L., Fu, L., Sun, J., Huang, Z., Fang, M., Zinkle, A., Liu, X., Lu, J., Pan, Z., Wang, Y., et al. (2023). Structural basis for FGF hormone signalling. Nature *618*, 862–870. https://doi.org/10.1038/s41586-023-06155-9.
17. Schlessinger, J., Plotnikov, A.N., Ibrahimi, O.A., Eliseenkova, A.V., Yeh, B.K., Yayon, A., Linhardt, R.J., and Mohammadi, M. (2000). Crystal structure of a ternary FGF-FGFR-heparin complex reveals a dual role for heparin in FGFR binding and dimerization. Mol. Cell *6*, 743–750. https://doi.org/10.1016/s1097-2765(00)00073-3.
18. Ferguson, H.R., Smith, M.P., and Francavilla, C. (2021). Fibroblast Growth Factor Receptors (FGFRs) and Noncanonical Partners in Cancer Signaling. Cells *10*, 1201. https://doi.org/10.3390/cells10051201.
19. Yang, L., Zhou, F., Zheng, D., Wang, D., Li, X., Zhao, C., and Huang, X. (2021). FGF/FGFR signaling: From lung development to respiratory diseases. Cytokine Growth Factor Rev. *62*, 94–104. https://doi.org/10.1016/j.cytogfr.2021.09.002.
20. Ruan, R., Li, L., Li, X., Huang, C., Zhang, Z., Zhong, H., Zeng, S., Shi, Q., Xia, Y., Zeng, Q., et al. (2023). Unleashing the potential of combining FGFR inhibitor and immune checkpoint blockade for FGF/FGFR signaling in tumor microenvironment. Mol. Cancer *22*, 60. https://doi.org/10.1186/s12943-023-01761-7.

21. Bogousslavsky, J., Victor, S.J., Salinas, E.O., Pallay, A., Donnan, G.A., Fieschi, C., Kaste, M., Orgogozo, J.M.M., Chamorro, A., and Desmet, A.; European-Australian Fiblast Trafermin in Acute Stroke Group (2002). Fiblast (trafermin) in acute stroke: results of the European-Australian phase II/III safety and efficacy trial. Cerebrovasc. Dis. *14*, 239–251. https://doi.org/10.1159/000065683.
22. Ardizzone, A., Bova, V., Casili, G., Filippone, A., Campolo, M., Lanza, M., Esposito, E., and Paterniti, I. (2022). SUN11602, a bFGF mimetic, modulated neuroinflammation, apoptosis and calcium-binding proteins in an in vivo model of MPTP-induced nigrostriatal degeneration. J. Neuroinflammation *19*, 107. https://doi.org/10.1186/s12974-022-02457-3.
23. Carter, E.P., Fearon, A.E., and Grose, R.P. (2015). Careless talk costs lives: fibroblast growth factor receptor signalling and the consequences of pathway malfunction. Trends Cell Biol. *25*, 221–233. https://doi.org/10.1016/j.tcb.2014.11.003.
24. Xie, Y., Su, N., Yang, J., Tan, Q., Huang, S., Jin, M., Ni, Z., Zhang, B., Zhang, D., Luo, F., et al. (2020). FGF/FGFR signaling in health and disease. Signal Transduct. Target. Ther. *5*, 181. https://doi.org/10.1038/s41392-020-00222-7.
25. Warkentin, T.E. (2022). Platelet-activating anti-PF4 disorders: An overview. Semin. Hematol. *59*, 59–71. https://doi.org/10.1053/j.seminhematol.2022.02.005.
26. Schroer, A.B., Ventura, P.B., Sucharov, J., Misra, R., Chui, M.K.K., Bieri, G., Horowitz, A.M., Smith, L.K., Encabo, K., Tenggara, I., et al. (2023). Platelet factors attenuate inflammation and rescue cognition in ageing. Nature *620*, 1071–1079. https://doi.org/10.1038/s41586-023-06436-3.
27. Pilatova, K., Greplova, K., Demlova, R., Bencsikova, B., Klement, G.L., and Zdrazilova-Dubska, L. (2013). Role of platelet chemokines, PF-4 and CTAP-III, in cancer biology. J. Hematol. Oncol. *6*, 42. https://doi.org/10.1186/1756-8722-6-42.
28. Koenen, R.R., von Hundelshausen, P., Nesmelova, I.V., Zernecke, A., Liehn, E.A., Sarabi, A., Kramp, B.K., Piccinini, A.M., Paludan, S.R., Kowalska, M.A., et al. (2009). Disrupting functional interactions between platelet chemokines inhibits atherosclerosis in hyperlipidemic mice. Nat. Med. *15*, 97–103. https://doi.org/10.1038/nm.1898.
29. Deng, T., Liu, Y., Gael, A., Fu, X., Deng, X., Liu, Y., Wu, Y., Wu, Y., Wang, H., Deng, Y., et al. (2022). Study on Proteomics-Based Aortic Dissection Molecular Markers Using iTRAQ Combined With Label Free Techniques. Front. Physiol. *13*, 862732. https://doi.org/10.3389/fphys.2022.862732.
30. Houard, X., Touat, Z., Ollivier, V., Louedec, L., Philippe, M., Sebbag, U., Meilhac, O., Rossignol, P., and Michel, J.B. (2009). Mediators of neutrophil recruitment in human abdominal aortic aneurysms. Cardiovasc. Res. *82*, 532–541. https://doi.org/10.1093/cvr/cvp048.
31. Li, X., Peng, X., Zoulikha, M., Boafo, G.F., Magar, K.T., Ju, Y., and He, W. (2024). Multifunctional nanoparticle-mediated combining therapy for human diseases. Signal Transduct. Target. Ther. *9*, 1. https://doi.org/10.1038/s41392-023-01668-1.
32. Xiao, L., Feng, M., Chen, C., Xiao, Q., Cui, Y., and Zhang, Y. (2023). Microenvironment-Regulating Drug Delivery Nanoparticles for Treating and Preventing Typical Biofilm-Induced Oral Diseases. Adv. Mater. *24*, e2304982. https://doi.org/10.1002/adma.202304982.
33. Sela, M., Poley, M., Mora-Raimundo, P., Kagan, S., Avital, A., Kaduri, M., Chen, G., Adir, O., Rozencweig, A., Weiss, Y., et al. (2023). Brain-Targeted Liposomes Loaded with Monoclonal Antibodies Reduce Alpha-Synuclein Aggregation and Improve Behavioral Symptoms in Parkinson's Disease. Adv. Mater. *35*, e2304654. https://doi.org/10.1002/adma.202304654.
34. Yang, X., Xu, C., Yao, F., Ding, Q., Liu, H., Luo, C., Wang, D., Huang, J., Li, Z., Shen, Y., et al. (2023). Targeting endothelial tight junctions to predict and protect thoracic aortic aneurysm and dissection. Eur. Heart J. *44*, 1248–1261. https://doi.org/10.1093/eurheartj/ehac823.
35. Luo, S., Kong, C., Zhao, S., Tang, X., Wang, Y., Zhou, X., Li, R., Liu, X., Tang, X., Sun, S., et al. (2023). Endothelial HDAC1-ZEB2-NuRD Complex Drives Aortic Aneurysm and Dissection Through Regulation of Protein S-Sulfhydration. Circulation *147*, 1382–1403. https://doi.org/10.1161/circulationaha.122.062743.
36. Pan, L., Lin, Z., Tang, X., Tian, J., Zheng, Q., Jing, J., Xie, L., Chen, H., Lu, Q., Wang, H., et al. (2020). S-Nitrosylation of Plastin-3 Exacerbates Thoracic Aortic Dissection Formation via Endothelial Barrier Dysfunction. Arterioscler. Thromb. Vasc. Biol. *40*, 175–188. https://doi.org/10.1161/atvbaha.119.313440.
37. Sachais, B.S., Turrentine, T., Dawicki McKenna, J.M., Rux, A.H., Rader, D., and Kowalska, M.A. (2007). Elimination of platelet factor 4 (PF4) from platelets reduces atherosclerosis in C57Bl/6 and apoE-/- mice. Thromb. Haemost. *98*, 1108–1113.
38. Yu, G., Rux, A.H., Ma, P., Bdeir, K., and Sachais, B.S. (2005). Endothelial expression of E-selectin is induced by the platelet-specific chemokine platelet factor 4 through LRP in an NF-kappaB-dependent manner. Blood *105*, 3545–3551. https://doi.org/10.1182/blood-2004-07-2617.
39. Aidoudi, S., and Bikfalvi, A. (2010). Interaction of PF4 (CXCL4) with the vasculature: a role in atherosclerosis and angiogenesis. Thromb. Haemost. *104*, 941–948. https://doi.org/10.1160/th10-03-0193.
40. El-Hamamsy, I., and Yacoub, M.H. (2009). Cellular and molecular mechanisms of thoracic aortic aneurysms. Nat. Rev. Cardiol. *6*, 771–786. https://doi.org/10.1038/nrcardio.2009.191.
41. Xu, K., Xu, C., Zhang, Y., Qi, F., Yu, B., Li, P., Jia, L., Li, Y., Xu, F.J., and Du, J. (2018). Identification of type IV collagen exposure as a molecular imaging target for early detection of thoracic aortic dissection. Theranostics *8*, 437–449. https://doi.org/10.7150/thno.22467.
42. Sulpice, E., Bryckaert, M., Lacour, J., Contreres, J.O., and Tobelem, G. (2002). Platelet factor 4 inhibits FGF2-induced endothelial cell proliferation via the extracellular signal-regulated kinase pathway but not by the phosphatidylinositol 3-kinase pathway. Blood *100*, 3087–3094. https://doi.org/10.1182/blood.V100.9.3087.
43. Perollet, C., Han, Z.C., Savona, C., Caen, J.P., and Bikfalvi, A. (1998). Platelet factor 4 modulates fibroblast growth factor 2 (FGF-2) activity and inhibits FGF-2 dimerization. Blood *91*, 3289–3299.
44. Singh, A., Ghosh, R., Asuru, T.R., Prajapat, S.K., Joshi, G., Gaur, K.K., Shrimali, N.M., Ojha, A., Vikram, N.K., Poncz, M., et al. (2024). Inhibition of cellular activation induced by platelet factor 4 via the CXCR3 pathway ameliorates Japanese encephalitis and dengue viral infections. J. Thromb. Haemost. *22*, 818–833. https://doi.org/10.1016/j.jtha.2023.11.015.
45. Petrai, I., Rombouts, K., Lasagni, L., Annunziato, F., Cosmi, L., Romanelli, R.G., Sagrinati, C., Mazzinghi, B., Pinzani, M., Romagnani, S., et al. (2008). Activation of p38(MAPK) mediates the angiostatic effect of the chemokine receptor CXCR3-B. Int. J. Biochem. Cell Biol. *40*, 1764–1774. https://doi.org/10.1016/j.biocel.2008.01.008.
46. Li, S., Xiong, N., Peng, Y., Tang, K., Bai, H., Lv, X., Jiang, Y., Qin, X., Yang, H., Wu, C., et al. (2018). Acidic pHe regulates cytoskeletal dynamics through conformational integrin β1 activation and promotes membrane protrusion. Biochim. Biophys. Acta, Mol. Basis Dis. *1864*, 2395–2408. https://doi.org/10.1016/j.bbadis.2018.04.019.
47. Wang, J., Tan, X., Guo, Q., Lin, X., Huang, Y., Chen, L., Zeng, X., Li, R., Wang, H., and Wu, X. (2020). FGF9 inhibition by a novel binding peptide has efficacy in gastric and bladder cancer per se and reverses resistance to cisplatin. Pharmacol. Res. *152*, 104575. https://doi.org/10.1016/j.phrs.2019.104575.

STAR★METHODS

KEY RESOURCES TABLE

REAGENT or RESOURCE	SOURCE	IDENTIFIER
Antibodies		
GAPDH Polyclonal antibody	Proteintech	RRID: AB_2263076
HRP-conjugated Affinipure Goat Anti-Rabbit IgG	Proteintech	RRID: AB_2722564
Phospho-p44/42 MAPK (Erk1/2)	Cell Signaling Technology	RRID: AB_2315112
p44/42 MAPK (Erk1/2)	Cell Signaling Technology	RRID: AB_3661799
Phospho-p38 MAPK Antibody	Cell Signaling Technology	RRID: AB_331641
p38 MAPK Rabbit mAb	Cell Signaling Technology	RRID: AB_10999090
Phospho-Akt(Ser473) Rabbit mAb	Cell Signaling Technology	RRID: AB_2315049
Phospho-Akt(Thr308) Rabbit mAb	Cell Signaling Technology	RRID: AB_331163
Akt Antibody	Cell Signaling Technology	RRID: AB_329827
Rabbit monoclonal antibody to CD31	Abcam	RRID: AB_2905525
Goat Anti-Rabbit IgG H&L (Alexa Fluor® 555)	Abcam	RRID: AB_2722519
DAPI Staining Solution	Abcam	RRID: AB_3661805
Bacterial and virus		
DH5-alpha competent *E. coli*	This paper	NA
Chemicals, peptides, and recombinant proteins		
3-Aminopropionitrile fumarate salt	Sigma-Aldrich	A3134
Angiotensin II	MedChemExpress	HY-13948
TNF-alpha	MedChemExpress	HY-P78218
SUN11602	MedChemExpress	Y-101493
Recombinant Human CXCL4	novoprotein	Cat. No.:CJ27
Heparinase III	Sigma-Aldrich	H8891
Critical commercial assays		
Cell Counting Kit-8	Dojindo	Cat:CK04
Mouse PF4 ELISA Kit	Abcam	Ab202403
Gelatin Zymography Analysis Kit	Real-Jimer	Ver. 740464
Deposited data		
RNAseq data	NIH SRA public database	PRJNA1126180
Experimental models: Cell lines		
human aortic endothelial cells	Pricella	Cat# CP-H080
Experimental models: Organisms/strains		
C57BL/6J mice	Medical Experimental Animal Center of Guangdong Province	NA
Software and algorithms		
GraphPad Prism	GraphPad Software, LLC	V9
Fiji ImageJ software	ImageJ.org	V1.53

EXPERIMENTAL MODEL AND PARTICIPANT DETAILS

Animals

All animal procedures were approved by the Ethics Committee of Guangdong People's Hospital, and all animal experiments were conducted in compliance with the National Institutes of Health Guidelines. Wild-type male C57BL/6J mice used in this study were purchased from the

Medical Experimental Animal Center of Guangdong Province. Throughout the experimental period, the mice were housed in an SPF environment. The temperature was maintained between 22°C and 24°C, humidity of 50–70%, and a 12 h dark/light cycle. For the β-aminopropionitrile monofumarate (BAPN) united Ang II –induced TAAD model, four-week-old mice with BAPN for 21 days and 7 days with AngII to investigate the potential effect of PF4 on the progression of TAAD. For the β-aminopropionitrile monofumarate (BAPN)–induced TAAD model, three-week-old male C57BL/6J mice were fed a normal diet and administered freshly prepared BAPN (Sigma-Aldrich, USA) solution dissolved in drinking water (250 μg/kg/day) for consecutive 25 days. The animals in this study were divided into five treatment groups: saline + BAPN, liposome + BAPN, PF4 + BAPN, Lipo-PF4 + BAPN, and Lipo-PF4 + SUN11602 (FGF mimic) + BAPN. All solutions were injected into the tail vein every three days, beginning three days before BAPN administration. Additionally, the same-aged male mice fed with a regular diet and drinking water were served as controls. At the end of the experiment, all mice were euthanized using an excess of 1% pentobarbital sodium, followed by decapitation. Aortic diameters were measured using a Vernier caliper.

In order to explore the mechanism of Lipo-PF4 for TAAD, we added another three group mice for mRNA sequencing list as follows: BAPN group: three-week-old mice were treated with 0.25% BAPN for 14 days; Lipo-PF4+BAPN group: three-week-old mice were treated with Liposome-PF4 once every three days. Three days after the first administration, mice were treated with 0.25% BAPN for 14 days. FGFR inhibitor +BAPN group: three-week-old mice were treated with 10 mg/kg AZD4547 once every two days. Two days after the first administration, mice were treated with 0.25% BAPN for 14 days.

Cells

Primary HAECs were purchased from Procell (Cat# CP-H080) and cultured in endothelial cell medium (ScienCell, Cat No. 1001) containing 10% FBS, 100 U/mL of penicillin, and 100 μg/mL streptomycin. Cells were cultured in a humidified incubator at 37°C and 5% CO2. The media was changed every two days. For the PF4 treatment experiments, HAECs were treated with an appropriate concentration of PF4 (Novoprotein, CJ27). Simultaneously, the cells were stimulated with Ang II (MedChemExpress, HY-13948) or TNFα (MedChemExpress, HY-P78218) for 36 h. In addition, HAECs were treated with PF4 and either Ang II or TNFα, along with HS-cleaving heparinase III (HSase). Furthermore, SUN11602 (MedChemExpress, HY-101493), an analog of FGF, was used to validate the mechanism of PF4.

METHOD DETAILS

Cell proliferation and adhesion assays

HAECs proliferation was determined using the CCK8 assay with a Cell Counting Kit-8 (DOJINDO, Cat. No: CK04) following the manufacturer's protocol. HAECs adhesion assay was performed according to a previously published protocol.[46] Briefly, HAECs were washed, trypsinized, and resuspended in the culture medium. HAECs were then added to each well and incubated for 48 h. Non-adherent cells were washed with PBS.

Cell migration assay

The invasive ability of HAECs was evaluated using Transwell chambers (BD Biosciences, 353097). Briefly, HAECs were suspended in a serum-free culture medium and placed in the upper chamber. The lower compartment contained a chemoattractant. The cells were then incubated for 12 h. Cells that migrated to the lower chamber were fixed and stained. Stained cells were counted under a microscope in five fields per well.

Tube formation assay

HAECs were suspended in a medium containing PF4 and either Ang II or TNFα. and seeded onto a 24-well plate pre-coated with Matrigel (BD, 354230). Following a 4-h incubation at 37°C, HAECs were stained with Calcein AM for 30 min. Images of tube formation were acquired using an inverted microscope. Tube formation was evaluated by analyzing the vessel area, junction, and vessel length using ImageJ software.

ELISA assays

PF4 levels were measured using a colorimetric ELISA kit (Abcam, ab202403) following the manufacturer's instructions. Briefly, the sample was mixed with diluent buffer at room temperature for 1 h on a plate shaker at 400 rpm. TMB substrate was added and incubated for 10 min in the dark. The OD was measured at 450 nm after adding the stop solution to each well.

Platelet factor 4 protein expression and purification

E. coli was used to express the PF4 protein. The generated pET28-His6-PF4 construct contained an IPTG-inducible His6-PF4. IPTG was added to stimulate the cells to express the corresponding proteins for several hours. The cells were then collected by centrifugation. The proteins were purified using nickel-based affinity chromatography, which involved the use of a hexahistidine (His6) affinity tag. The His6 tag binds to metal ions, such as nickel (Ni2+), which enables the separation of His6-PF4 from all other proteins in the cell. After lysing the cells to release the protein, His6-tagged proteins were extracted using a nickel column. The purity of the His6-PF4 protein was evaluated by SDS-PAGE gel.

Preparation and property analysis of liposomes

The thin-film hydration method was used to prepare PF4-loaded liposomes (Lipo-PF4). Lipo-PF4 was prepared by dissolving DOPC, cholesterol, and DSPE-PEG2000 in chloroform. Methanol was added to chloroform in a 1:3 volume ratio. The mixture was then evaporated using a rotary evaporator at room temperature with a rotation speed of 100 rpm for 3 h. Next, a thin layer of the Lipo-PF4 film was obtained. The dried thin films were hydrated with PF4 in PBS and sonicated. The extra solution was centrifuged at 15000 × g at 4°C for 15 min. The liposome solution was filtered to obtain Lipo-PF4. We used the dynamic light-scattering method with a fiber-optics particle analyzer (FPAR-1000, Otsuka Electronics Co., Ltd, Osaka, Japan) to determine the particle size of Lipo-PF4. The morphology and diameter of Lipo-PF4 were observed using an electron microscope.

Histological and immunofluorescence staining

The aortic tissue was fixed overnight in 4% PFA, dehydrated, and embedded in paraffin. Aortic tissue sections (3 μm) were deparaffinized and rehydrated. The pathological condition of the aorta was assessed by staining with hematoxylin and eosin (H&E), Masson, and Verhoeff's elastic (EVG) using commercial kits, following the manufacturer's instructions (1, no elastin degradation; 2, mild; 3, moderate; and 4, severe elastin degradation). For immunofluorescence analysis, mouse aortic endothelial cells were incubated overnight with primary antibodies against CD31 (Abcam, ab222783, 1:200) at 4°C in a wet box, followed by incubation with a secondary antibody (Abcam, ab150078, 1:1000) at room temperature for 1 h. Cell nuclei were stained with 4′,6-diamidino-2-phenylindole (DAPI) (Abcam, ab228549, UK). Images were acquired using a confocal microscope.

Gelatin zymography

To analyze the activity of matrix metalloproteinase, the cultured supernatant of vascular wall endothelial cells was loaded onto gelatin gels and subjected to electrophoresis. The Gelatin-Zymography Kit (RTD6143; Real-Jimer, Beijing, China) was used to detect MMP activity following the manufacturer's protocol.

RNA sequencing

The blood vessels of mice (BAPN group; Lipo-PF4+BAPN group; FGFR inhibitor +BAPN group) were repeatedly washed with D-Hank's solution to remove residual blood. Peel off the adipose tissue and small blood vessels outside the aorta, and carefully peel off the adventitia until the blood vessels are smooth and transparent. The aorta was placed in DMEM solution (containing 4.5 g/L glucose, 10 mmol/L pyruvate, 2 mmol/L glutamine, 100 U/L penicillin and streptomycin, 20% fetal bovine serum), the aorta was cut longitudinally with an ophthalmic scissor, and the intima was lightly scraped three times with a sterile blade. The intimal tissue was collected by centrifugation. Individual endothelial cells were isolated by combined trypsin-collagenase digestion. Finally, CD31 flow antibody was used to isolate endothelial cells. Cell samples were used for RNA isolation with the Trizol Reagent (10296010, Invitrogen, CA, USA). Sequencing libraries were generated using the TruSeq RNA Sample Preparation Kit (Illumina, San Diego, CA, USA). All samples underwent Illumina Novaseq6000 sequencing (Kindstar Sequenon, Wuhan, China) with a paired-end 150 bp read length. Raw data of fastq format were nly processed through in-house perl scripts. In this step, clean data (clean reads) were obtained by removing reads containing adapter, reads containing ploy-N and low-quality reads from raw data. At the same time, Q20, Q30 and GC content the clean data were calculated. All the downstream analyses were based on the clean data with high quality. The clean reads were mapped to the GRCm38 mouse reference sequence. Differential expression analysis of two groups (three biological replicates per group) was performed using the DESeq2 R package (1.16.1). The resulting *p*-values were adjusted using the Benjamini and Hochberg's approach for controlling the false discovery rate. Genes with an adjusted *p*-value <0.05 found by DESeq2 were assigned as differentially expressed. GO enrichment analysis of differentially expressed genes was implemented by the clusterProfiler R package. GO terms with corrected *p* value less than 0.05 were considered significantly enriched by differential expressed genes. The transcriptome sequencing data of all the samples involved in this study have been uploaded to the SRA public database with accession number PRJNA11261800(N: BAPN group; P: Lipo-PF4+BAPN group; I: FGFR inhibitor+ BAPN group).

Western blot

Western blotting was performed according to a previously described protocol.[47] The cells were lysed using 1× SDS–PAGE loading buffer. Equal amounts of protein extracts were separated using 10% SDS–PAGE gels and transferred to a PVDF membrane. After blocking with 5% BSA for 1 h, the membranes were incubated overnight at 4°C with primary antibodies (GAPDH, Proteintech, 10494-1-AP, 1:4000; Phospho-Erk1/2, CST, #4370, 1:2000; Total-Erk1/2, CST, #4695, 1:2000; Phospho-P38, CST, #9211, 1:2000; Total-P38, CST, #8690, 1:2000; Phospho-Akt [Ser473], CST, #4060, 1:2000; Phospho-Akt [Thr308], CST, #13038, 1:2000; Total-Akt, CST, #9272, 1:2000). Membranes were then incubated with secondary antibodies at room temperature for 1 h. The blots were detected using an enhanced chemiluminescence (ECL) kit and measured using Image 500.

QUANTIFICATION AND STATISTICAL ANALYSIS

Continuous data are presented as mean ± SEM. Categorical data are presented as numbers and percentages (%). Shapiro-Wilk tests were performed to assess the normality of the data distribution, and the Brown–Forsythe test was used to check for equal variances among

normally distributed data. Comparisons between groups were analyzed using Student's t-test or one-way ANOVA, depending on the normal distribution of the data and equality of variances. Non-parametric tests were performed for data that did not follow a normal distribution. Comparisons between two groups were performed using the Mann–Whitney test or Kruskal–Wallis test with Dunn's multiple comparison test. The "n" in the figure legends represents biological replicates. A p value of <0.05 was considered significant in all statistical comparisons. All statistical analyses were performed using GraphPad Prism version 9.0.1.